Published in final edited form as:
J Comput Assist Tomogr. 2012 ; 36(1): 77–82. doi:10.1097/RCT.0b013e3182388cdf.

Peripheral Artery Wall Imaging Using Contrast-Enhanced, Susceptibility Weighted Phase Imaging

Qi Liu, MS[1,2], **Zhaoyang Fan, PhD**[1,2], **Qi Yang, MD**[3], and **Debiao Li, PhD**[1,2]

[1]Biomedical Imaging Research Institute, Department of Biomedical Sciences, Cedars-Sinai Medical Center, Los Angeles, CA, USA

[2]Departments of Biomedical Engineering and Radiology, Northwestern University, Chicago, IL, USA

[3]Department of Radiology, Xuanwu Hospital, Beijing, China

Abstract

Purpose—To demonstrate improved delineation of peripheral artery wall in susceptibility weighted imaging (SWI) phase images by utilizing gadolinium contrast agent.

Materials and methods—Superficial femoral arteries were imaged using high resolution SWI in 11 healthy volunteers before, and after injection of gadopentetate dimeglumine. Two post-contrast scans started 1 min and 11 mins after injection respectively. Eight out of the 11 volunteers also underwent double-inversion-recovery (DIR) turbo-spin-echo (TSE) scans. The same resolution and matrix size were used between SWI and TSE studies, and TSE locations were matched to SWI images. Arterial lumen-wall phase difference and phase contrast-to-noise ratio (CNR) were measured and compared between pre- and post-contrast SWI measurements. The lumen and wall areas measured on both TSE and matching SWI images were respectively analyzed for agreement. Another 2 volunteers participated in a double-echo gradient-echo study. Results were compared to SWI.

Results—By injecting gadolinium contrast agent, phase difference changed by 54.5% and −1.6%, and phase CNR changed by 85.7% and 27.0%, for the 1st and 2nd post-contrast scans respectively. Morphological measurements showed insignificant difference between TSE and SWIs based on paired t-tests; good agreements in Bland-Altman plots were achieved. The double-echo gradient-echo study had similar phase measurements as SWI.

Conclusion—Contrast-enhanced phase imaging improves artery wall delineation in SWI of peripheral artery wall. Contrast-enhanced SWI is a promising vessel wall imaging technique.

Keywords

susceptibility weighted imaging; phase imaging; susceptibility; gadolinium contrast agent

Introduction

Atherosclerosis is a systemic disease manifesting as arterial wall thickening and responsible for thromboembolic cerebral infarction, thrombotic myocardial infarction, and peripheral arterial disease (PAD), a vascular disorder often involving the lower extremities. Currently PAD affects approximately 8 million people in the United States, and 12% to 20% of

Corresponding Author (Reprint Info): Debiao Li, Ph.D., Biomedical Imaging Research Institute, Cedars-Sinai Medical Center, Davis Building, Suite G-140, 8700 Beverly Blvd., Los Angeles, CA 90048., Phone: 310-423-7743, Fax: 310-967-0639, debiaoli@gmail.com.

Americans over 65 years of age (1). PAD is found to be a marker for systemic atherosclerotic disease (2). It is associated with morbidity, impaired quality of life, or even death. In addition to the degree of lumen stenosis, imaging of vessel wall is essential in assessing risks associated with PAD, since atherosclerotic plaque vulnerability depends on its morphology and composition (3–5). Major challenges for peripheral artery wall imaging are the relatively slow blood flow and the need to cover large volume of interest. Therefore, a three dimensional (3D) imaging method with good artery lumen-wall contrast even at slow or regurgitating flow situation is desired.

Yang et al. demonstrated the feasibility of using fully flow-compensated high-resolution susceptibility weighted imaging (SWI) sequence to image superficial femoral arterial wall morphology and plaque calcification without the need to suppress the signal from blood (6). The contrast mechanism between the wall and lumen on phase image was attributed to susceptibility difference between these two regions. At 3.0 Tesla, a long echo time of 15.6 ms was used to enhance phase difference. Because the lumen-wall contrast in a phase image appeared more pronounced than in a magnitude image, the delineation of arterial wall boundaries was better achieved in phase image. Despite the benefits of SWI vessel wall imaging, namely blood flow independence, three dimensional coverage, and sensitivity to calcification, the limited contrast-to-noise-ratio (CNR) is still a problem affecting visualization of wall boundaries.

In this work, we proposed to utilize gadolinium (Gd) contrast agent to alter blood and vessel wall susceptibility and thus to enhance the lumen-wall contrast in SWI phase images. The benefit of this contrast-enhanced method was verified on volunteer femoral arteries by comparison with pre-contrast SWI. The results were also compared to a double-echo gradient-echo (GRE) study. To examine the accuracy in morphological measurement, pre-contrast SWI was compared with the reference method in vessel wall imaging, single slice DIR TSE, in measuring femoral artery lumen and wall area.

Materials and Methods

Imaging Protocols

Eleven volunteers (age 53.2±6.4 years) participated in the study on a 3.0 Tesla system (Tim Trio, Siemens, Erlangen, Germany) using a 6-channel body matrix and spine coils. The study was approved by our Institutional Review Board and informed consent was obtained from all volunteers. Following a vessel scout, a multi-slice time-of-flight angiography scan was used to identify the location of femoral bifurcation. The imaging volume of 3D SWI was then placed approximately 1 cm below the bifurcation.

The commercial SWI sequence (essentially a long TE, flow-compensated spoiled gradient echo) was used with parameters similar to previous publication (6): TR/TE = 26.0/15.6 ms, FOV = 186×230 mm^2, matrix = 260×320, 32 slices, spatial resolution = 0.72×0.72×2.0 mm^3, acquisition time = 4.1 min, flip angle = 15°, bandwidth = 80 Hz/pixel, transverse acquisition. A single injection of 0.1 mmol/kg bodyweight gadopentetate dimeglumine (Magnevist, Bayer Healthcare, Wayne, NJ) was administered IV at a rate of 2 ml/sec. Two SWI scans were performed 1 min (named '1st contrast-enhanced' hereafter) and 11 min (named '2nd contrast-enhanced' hereafter) after contrast injection respectively, with the same parameters as in the pre-contrast scan.

Eight among the 11 volunteers also participated in comparative TSE study before contrast injection. Three slices from the top, middle, and bottom of the SWI imaging volume in each volunteer were selected for single-slice T2-weighted DIR-TSE scans with the same FOV, resolution, and slice thickness. Other parameters were: TE=51–52 ms, TR= 4000 ms, flip angle=180°, 2 averages, acquisition time= 2.6 mins, bandwidth=260–270 Hz/pixel, spectrally selective fat saturation. Concerning the relative weak flow pulsatility in femoral artery, no ECG gating was used according to literature (7).

To access the accuracy of SWI phase measurement, it was compared to results of a double-echo GRE study. The sequence was modified by adding a second echo in the SWI sequence, and imaging parameters were the same as SWI except the following: TR/TE1/TE2 = 43.0/11.25/21.8 ms, bandwidth = 120 Hz/pixel, and acquisition time = 6.4 min. The same Gd contrast agent dosage and injection scheme as the SWI study was used, followed by two back-to-back double-echo GRE acquisitions, each lasting 6.4 minutes. 2 volunteers participated in this study.

Data Analysis

High-pass filtering was performed on the complex raw image following SWI acquisition to eliminate B_0 field inhomogeneity and to keep mainly signals caused by local susceptibility variation. Then the phase signal as an image was used for vessel wall delineation and data analysis. The high-pass filtering process involved dividing the original complex raw image over its low-pass filtered image. Low-pass filtering was achieved by a Hanning filter with size of 96×96.

In contrast-enhanced SWI studies, the central 20 slices were analyzed. For each volunteer, the angle between long-axis of the selected femoral artery segment and the static magnetic field θ (range: 9.2°–20.4°) was first calculated by measuring time-of-flight (TOF) maximum-intensity-projection (MIP) images. This angle was later used to adjust for geometric factor’s effect on susceptibility induced phase as a function of blood vessel orientation (8). All phase images were inverted for better visualization. In phase images, region-of-interests (ROIs) were drawn manually in lumen and wall area of the femoral artery, ensuring inclusion of relatively homogeneous regions. ROIs were then copied to corresponding magnitude images. Images were analyzed on a workstation (Leonardo, Siemens).

Phase contrast was defined as the phase difference between lumen and wall:

$$\Delta\phi=\phi_{\mathrm{lumen}} - \phi_{\mathrm{wall}} \quad [1]$$

where ϕ_{lumen} is the average phase value within the ROI in the lumen, and ϕ_{wall} is that in the wall. In a simplified blood vessel model (8), induced magnetic field and thus accumulated phase has strong dependence on the angle θ between blood vessel and static magnetic field B_0. This effect is accounted for by modifying equation [1] into:

$$\Delta\phi=(\phi_{\mathrm{lumen}} - \sigma_{\mathrm{wall}}) \times 2/(3\cos^2\theta - 1) \quad [2]$$

The adjusted phase contrast equals the phase difference as if the vessel segment was aligned with B_0.

Phase contrast-to-noise ratio (CNR) was defined as

$$\mathrm{CNR}_{\mathrm{phase}}=\Delta\phi \times \mathrm{SNR}_{\mathrm{magnitude}} \quad [3]$$

$SNR_{magnitude}$ was measured on magnitude images as the average pixel intensity in wall area over noise standard deviation measured in an anatomical free region (6). Paired t-tests were used to identify any changes in phase contrast and CNR_{phase}.

Morphology measurements of vessel lumen and wall area were performed using public-domain image processing software (Image J, version 1.40g, National Institutes of Health, USA). Lumen and wall contours were manually drawn by an experienced researcher on matched pre- and post-contrast SWI images and single-slice DIR-TSE images separately for the 8 volunteers. Paired t-tests were used to identify any difference between each pair of TSE and SWI images, and Bland-Altman plots were made to show agreement between measurements. All statistical tests were performed at α=0.05, using SPSS v. 16.0 (SPSS, Chicago, IL).

Many sources contribute to magnetic field inhomogeneity, including magnetic susceptibility (ΔB_{suscep}), chemical shift (ΔB_{cs}), global geometry ($\Delta B_{global\ geometry}$), and inhomogeneity produced by scanner hardware ($\Delta B_{main\ field}$) (8). Injecting Gd contrast also leads to field change (ΔB_{Gd}) in addition to ΔB_{suscep}.

Before Gd injection, phase (ϕ_{pre}) should be written as:

$$\phi_{pre}=-\gamma\,(\Delta B_{suscep}+\Delta B_{cs}+\Delta B_{global\ geometry}+\Delta B_{main\ field})\,TE+\phi_0 \quad [4]$$

where TE is time-of-echo, γ is gyromagnetic ratio, ϕ_0 is phase offset.

In SWI the high-pass filtering procedure can largely remove $\Delta B_{global\ geometry}$ and $\Delta B_{main\ field}$.

To accurately quantify Gd-induced field change, complex dividing GRE images before and after Gd injection was calculated.

After Gd injection phase (ϕ_{post}) should be written as:

$$\phi_{post}=-\gamma\,(\Delta B_{suscep}+\Delta B_{cs}+\Delta B_{global\ geometry}+\Delta B_{main\ field}+\Delta B_{Gd})\,TE+\phi_0 \quad [5]$$

Subtracting equation [5] from [4], we have:

$$\phi_{pre}-\phi_{post}=\gamma\,\Delta B_{Gd}\,TE \quad [6]$$

and the Gd-induced magnetic susceptibility $\Delta\chi_{Gd}$ is:

$$\Delta\chi_{Gd}=(\phi_{pre}-\phi_{post})/(\gamma B_0 TE) \quad [7]$$

$\Delta\chi_{Gd}$ can be calculated if phase difference of pre and post images and TE are known. Geometry effect was ignored.

In each volunteer, pre and post phase difference was measured for lumen and wall areas each in 4 to 6 selected ROIs, and then divided by γB_0TE. This is done for both 1st and 2nd post-contrast acquisitions. Data was averaged between echoes, ROIs and volunteers.

Results

Comparison between pre-contrast and contrast-enhanced SWI phase images revealed that both contrast-enhanced images had improved vessel wall delineation, and the 1st contrast-enhanced SWI showed more pronounced improvement in delineation than the 2nd one. Representative images were shown in Figs. 1 and 2. Results of quantitative analyses on $\Delta\phi$ and CNR_{phase} were shown in Table 1. Paired t-tests revealed that $\Delta\phi$ is significantly different between pre-contrast and 1st contrast-enhanced images, and CNR_{phase} is significantly different between the pre-contrast scan and both of the contrast-enhanced scans. For the 1st contrast-enhanced SWI, this amounted to an increase of 54.5% in $\Delta\phi$ and 85.7% increase in CNR phase. For the 2nd contrast-enhanced SWI, though no statistically significant difference in $\Delta\phi$ (1.6% decrease) was identified, CNR_{phase} increased by 27.0%.

Representative images were shown in Fig. 3 to demonstrate similarity in morphology in TSE and SWIs images. Paired t-tests revealed no significant difference in lumen and wall area measurements between TSE and any SWI. For lumen and wall measurements, p-values were 0.618 and 0.351, 0.818 and 0.619, and 0.841 and 0.693, respectively, between TSE and pre-contrast SWI, 1st and 2nd contrast-enhanced SWIs. Bland-Altman plots showed that there was good agreement in morphological measurements made from TSE and SWI images (Fig. 4).

The average lumen $\Delta\chi_{Gd}$ were 0.32ppm (in SI units) and 0.22ppm, and the average wall $\Delta\chi_{Gd}$ were 0.20ppm and 0.25ppm, respectively, for the 1st and 2nd contrast-enhanced double-echo GRE acquisitions. If these susceptibility values were translated into SWI (with TE of 15.6ms) phase values, the lumen and wall would change by 36.5° and 22.3°, and by 25.1° and 28.5°, respectively, in the 1st and 2^{nd} contrast-enhanced images. Thus it was expected that SWI lumen-wall $\Delta\phi$ would change by 14.2 ° and by −3.43 ° in the 1st and 2nd contrast-enhanced images respectively.

Discussion

Conventional multi-contrast multi-slice 2D TSE imaging has been a ‘standard’ technique to image vessel wall and atherosclerotic plaques (9). However this technique has several major drawbacks: it is susceptible to wall-mimicking flow artifacts that may lead to misinterpretation; it requires relative long acquisition time to achieve sufficient SNR and resolution; it has limited coverage which restricts its clinical usefulness.

Various black blood MRI techniques that suppress the signal from flowing blood are employed for imaging of vessel wall to provide good wall conspicuity. Typical blood suppressing schemes include the use of radiofrequency pulses to pre-saturate inflow blood (10), the use of double inversion recovery (DIR) preparation to null signal from inflow blood following appropriate inversion time (11), or the use of flow-sensitive dephasing (FSD) preparation (12, 13). However, these techniques rely on blood flow to achieve black blood effects, which may result in residual luminal blood signal in areas with slow flow, and complex flow patterns in patients with severe atherosclerosis could deteriorate their efficacy. Plaque-mimicking flow artifacts may be misinterpreted as thickened vessel wall (14). Furthermore, inflow pre-saturation and DIR methods become unreliable when combined with large-coverage 3D vessel wall imaging (15). To overcome these limitations, several flow-independent blood suppression techniques were developed. T2-prepared inversion recovery (IR) sequence relies on difference in T1 and T2 between blood and the vessel wall to suppress blood (16), yet it is susceptible to heart rate variation and improper inversion time selection. Phase-sensitive IR was employed by Wang et al. to image carotid intraplaque hemorrhage, however blood suppression efficiency still depends on blood replenishment rate (17). Xie et al. incorporated steady-state free precession (SSFP) based phase-sensitive reconstruction in a T2-preapared non-selective IR method, yet additional acquisition was needed to resolve polarity information, resulting in prolonged imaging time (18).

SWI phase imaging of vessel wall was previously proposed, and here we showed that much better images can be produced using our contrast-enhanced method. Both SWI and contrast-enhanced SWI may offer some superiority when compared to TSE. The flow-insensitive nature of SWI technique is an advantage in atherosclerosis studies. Complex flow patterns (e.g. turbulent flow) in patients that often deteriorate conventional blood suppression techniques are less likely a problem for SWI techniques because of the flow-compensation gradients used. SWI also has the advantage of being sensitive to calcification. Previous studies have reported high correlation between calcification sizes measured on SWI and Computed Tomography (6). Yet the ability of using SWI to explore more complicated plaque composition needs further investigation. In fact, this is a challenging problem for both conventional SWI and the contrast-enhanced technique proposed here, since different plaque components can have distinct magnetic properties which complicate phase image contrast. A possible solution to this may involve quantitative susceptibility mapping techniques (19, 20) to resolve component specific susceptibility values. 3D imaging coverage achieved by SWI is also an important benefit given that 3D large-coverage of artery wall imaging have only been available recently (21). Compared to conventional SWI, increased phase CNR obtained in our contrast-enhanced SWI method leaves room to boost its applications by further improving spatial resolution, reducing imaging time or imaging at a lower magnetic field (e.g. 1.5 Tesla).

Though previous studies have shown improvement in contrast-enhanced SWI image quality in the brain (22–24), we have demonstrated for the first time the use of gadolinium contrast agent to enhance peripheral vessel wall in SWI. In fact the mechanism of improved image contrast in the arterial wall is different from that in the brain. In brain SWI, phase difference between venous blood and surrounding brain parenchyma within a single voxel leads to signal cancellation in magnitude, and this cancellation effect is further enhanced when magnitude is multiplied by a filter generated from modulated phase. The administration of Gd contrast agent alters venous blood susceptibility and lead to increased phase difference between blood and brain parenchyma; meanwhile venous blood magnetization is increased due to T1-shortening effect of Gd contrast agent. The combined effect of both increased phase difference and bigger blood magnetization accounts for the fact that small veins in the brain appear more pronounced in SWI (22).

Yet the mechanism is different in artery wall imaging using contrast-enhanced SWI phase images. Since tissue volume (e.g. lumen, wall, muscle) in and surrounding the vessel wall is relatively large and usually occupy at least tens of pixels, signal cancellation could only occur at the interface of different tissues, and hence is not of primary concern. In fact, the susceptibility differences between tissues are considered to be the main source of image contrast in a SWI phase image. This is because differences in susceptibility will result in differences in magnetic field strength (ΔB), and hence difference in phase (ϕ) as dictated by the equation $\phi = -\gamma \Delta B * TE$ (γ is the gyromagnetic ratio; TE is echo time). Since almost all human constituents are diamagnetic (25), tissues that are paramagnetic than water will have negative phase and vice versa.

Arterial blood is slightly paramagnetic, while artery wall is diamagnetic and appears bright in our pre-contrast phase image (please note that all phase images were inverted before display). This explains the $\Delta\phi$ of 25.7°±6.3° between lumen and wall in our pre-contrast phase image, which is close to 20.6°±2.9° as presented in previous literature (6). After Gd agent injection, magnetic susceptibility will change in both arterial lumen and wall. In the lumen, blood becomes more paramagnetic quickly through mixing volume of blood with paramagnetic Gd contrast agent solution, and then gradually returns to its normal susceptibility when Gd is washed-out. A similarly process also takes place in the arterial wall: paramagnetic Gd agent perfuses into the wall via vaso vasorum, making the wall less diamagnetic, and is then gradually washed-out. However, this process is much slower and susceptibility change is smaller when compared to the competing process in the lumen. During the acquisition of 1st contrast-enhanced SWI, the lumen susceptibility change is greater than that in the wall since lumen has faster wash-in, and $\Delta\phi$ between lumen and wall increases from 25.7°±6.3° (pre-contrast) to 39.7°±7.6°. During the acquisition of 2nd contrast-enhanced SWI when Gd agent in the lumen starts to wash-out while Gd concentration in the wall is still at its high, $\Delta\phi$ decreases and approaches its value before contrast injection, as shown by the similar $\Delta\phi$ between pre-contrast and 2nd contrast-enhanced SWI. In addition to its magnetic susceptibility property, Gd also has T1-shortening effect that increases SNR in magnitude image. During the acquisition of 1st contrast-enhanced SWI, Gd concentration and hence SNR magnitude is high in the blood, thus CNR_{phase} (recall in equation [3] that CNR_{phase} is the multiple of $\Delta\phi$ and $SNR_{magnitude}$) increases compared with pre-contrast. The 85.7% increase in CNR_{phase} is higher than the 54.5% increase in $\Delta\phi$. During the the acquisition of 2nd contrast-enhanced SWI, even though $\Delta\phi$ is about the same, increased SNR magnitude explains the 27.0% increase in CNR_{phase}.

From the above discussions, it is evident that the enhancement dynamics of gadolinium contrast agent in lumen and wall is an important factor. It is speculated that quantification of dynamic enhancement properties as reflected by SWI phase change could provide useful physiological or pathological knowledge, or even serving as an indicator to supplement atherosclerotic plaque component discrimination. Future studies exploiting phase enhancement properties of gadolinium contrast agent are advised to focus both on early and late stage effects.

The agreement between TSE and SWIs area measurements demonstrates the reliability of SWI phase image to serve as vessel wall imaging methods. The accurate lumen size measurement in SWI reflects its flow-insensitive nature. Nevertheless, when considering that artery wall has multiple structures including intima, media, and adventitia, it seems TSE and SWI image does not have to necessarily match in morphology when super high resolution is used. Higher resolution comparison studies between TSE and SWI are interesting future topics.

Based on $\Delta\chi_{Gd}$ values obtained by double-echo GRE imaging, it is predicted that the lumen-wall $\Delta\phi$ would change by 14.2°and −3.43°, respectively, in the 1st and 2nd contrast-enhanced SWI acquisitions, in general agreement with the lumen-wall $\Delta\phi$ changes of 14.0° and −0.4° measured in volunteer studies.

There are certain limitations in this study. Firstly, imaging protocol was not optimized after contrast injection. As a preliminary study, the aim was to demonstrate the feasibility to obtain improved wall delineation. Obviously there is still room to get improved image quality. This can be done by optimizing the timing between contrast injection and initiation of acquisition, by optimizing post-contrast sequence parameters such as TE and flip angle, or by optimizing k-space filling schemes (e.g. centric reordering). Secondly, partial volume problem, which was out of scope of this paper, was not addressed. Thirdly, this study mainly focused on technical development and failed to include patient population, which would have given more power to the usefulness of our method. Research on contrast-enhanced SWI studies involving patient with complicated atherosclerotic plaque components are underway.

In conclusion, combining gadolinium contrast agent injection and SWI phase imaging will result in better peripheral artery wall delineation. The 1st contrast-enhanced SWI is better than the 2nd contrast-enhanced SWI in terms of CNR_{phase}. The degree of delineation improvement depends on the time of acquisition, reflecting the pharmacodynamics difference of contrast agent in lumen and arterial wall enhancement. Lumen and wall area measurements made on SWIs and the 'gold standard' TSE images show no significant difference. Double-echo GRE study generally agreed with phase values measured on SWI.

Contrast-enhanced SWI phase imaging has the potential to be an alternative 3D flow-insensitive vessel wall technique for imaging of wall thickening.

Acknowledgments

Grant sponsors: National Institutes of Health (NIH); Grant number: 1R01HL096119

References

1. Ostchega Y, Paulose-Ram R, Dillon CF, Gu Q, Hughes JP. Prevalence of peripheral arterial disease and risk factors in persons aged 60 and older: data from the National Health and Nutrition Examination Survey 1999–2004. J Am Geriatr Soc. 2007; 55:583–589. [PubMed: 17397438]
2. Lloyd-Jones D, Adams RJ, Brown TM, et al. Heart disease and stroke statistics--2010 update: a report from the American Heart Association. Circulation. 2010; 121:e46–e215. [PubMed: 20019324]
3. Virmani R, Kolodgie FD, Burke AP, Farb A, Schwartz SM. Lessons from sudden coronary death: a comprehensive morphological classification scheme for atherosclerotic lesions. Arterioscler Thromb Vasc Biol. 2000; 20:1262–1275. [PubMed: 10807742]
4. Naghavi M, Libby P, Falk E, et al. From vulnerable plaque to vulnerable patient: a call for new definitions and risk assessment strategies: Part I. Circulation. 2003; 108:1664–1672. [PubMed: 14530185]
5. Saam T, Hatsukami TS, Takaya N, et al. The vulnerable, or high-risk, atherosclerotic plaque: noninvasive MR imaging for characterization and assessment. Radiology. 2007; 244:64–77. [PubMed: 17581895]
6. Yang Q, Liu J, Barnes SR, et al. Imaging the vessel wall in major peripheral arteries using susceptibility-weighted imaging. J Magn Reson Imaging. 2009; 30:357–365. [PubMed: 19629989]
7. Mani V, Itskovich VV, Aguiar SH, et al. Comparison of gated and non-gated fast multislice black-blood carotid imaging using rapid extended coverage and inflow/outflow saturation techniques. J Magn Reson Imaging. 2005; 22:628–633. [PubMed: 16215965]
8. Haacke EM, Mittal S, Wu Z, Neelavalli J, Cheng YC. Susceptibility-weighted imaging: technical aspects and clinical applications, part 1. AJNR Am J Neuroradiol. 2009; 30:19–30. [PubMed: 19039041]
9. Yuan C, Mitsumori LM, Beach KW, Maravilla KR. Carotid atherosclerotic plaque: noninvasive MR characterization and identification of vulnerable lesions. Radiology. 2001; 221:285–299. [PubMed: 11687667]
10. Felmlee JP, Ehman RL. Spatial presaturation: a method for suppressing flow artifacts and improving depiction of vascular anatomy in MR imaging. Radiology. 1987; 164:559–564. [PubMed: 3602402]
11. Edelman RR, Chien D, Kim D. Fast selective black blood MR imaging. Radiology. 1991; 181:655–660. [PubMed: 1947077]
12. Koktzoglou I, Li D. Diffusion-prepared segmented steady-state free precession: Application to 3D black-blood cardiovascular magnetic resonance of the thoracic aorta and carotid artery walls. J Cardiovasc Magn Reson. 2007; 9:33–42. [PubMed: 17178678]
13. Fan Z, Zhang Z, Chung YC, et al. Carotid arterial wall MRI at 3T using 3D variable-flip-angle turbo spin-echo (TSE) with flow-sensitive dephasing (FSD). J Magn Reson Imaging. 2010; 31:645–654. [PubMed: 20187208]
14. Steinman DA, Rutt BK. On the nature and reduction of plaque-mimicking flow artifacts in black blood MRI of the carotid bifurcation. Magn Reson Med. 1998; 39:635–641. [PubMed: 9543426]
15. Milner JS, Moore JA, Rutt BK, Steinman DA. Hemodynamics of human carotid artery bifurcations: computational studies with models reconstructed from magnetic resonance imaging of normal subjects. J Vasc Surg. 1998; 28:143–156. [PubMed: 9685141]
16. Liu CY, Bley TA, Wieben O, Brittain JH, Reeder SB. Flow-independent T(2)-prepared inversion recovery black-blood MR imaging. J Magn Reson Imaging. 2010; 31:248–254. [PubMed: 20027595]

17. Wang J, Ferguson MS, Balu N, Yuan C, Hatsukami TS, Bornert P. Improved carotid intraplaque hemorrhage imaging using a slab-selective phase-sensitive inversion-recovery (SPI) sequence. Magn Reson Med. 2010; 64:1332–1340. [PubMed: 20597120]

18. Xie J, Bi X, Fan Z, et al. 3D flow-independent peripheral vessel wall imaging using T2-prepared phase-sensitive inversion-recovery steady-state free precession. Journal of Magnetic Resonance Imaging. 2010; 32:399–408. [PubMed: 20677269]

19. Haacke EM, Tang J, Neelavalli J, Cheng YC. Susceptibility mapping as a means to visualize veins and quantify oxygen saturation. J Magn Reson Imaging. 32:663–676. [PubMed: 20815065]

20. de Rochefort L, Liu T, Kressler B, et al. Quantitative susceptibility map reconstruction from MR phase data using bayesian regularization: validation and application to brain imaging. Magn Reson Med. 63:194–206. [PubMed: 19953507]

21. Zhang Z, Fan Z, Carroll TJ, et al. Three-dimensional T2-weighted MRI of the human femoral arterial vessel wall at 3.0 Tesla. Invest Radiol. 2009; 44:619–626. [PubMed: 19692844]

22. Lin W, Mukherjee P, An H, et al. Improving high-resolution MR bold venographic imaging using a T1 reducing contrast agent. J Magn Reson Imaging. 1999; 10:118–123. [PubMed: 10441013]

23. Pinker K, Noebauer-Huhmann IM, Stavrou I, et al. High-field, high-resolution, susceptibility-weighted magnetic resonance imaging: improved image quality by addition of contrast agent and higher field strength in patients with brain tumors. Neuroradiology. 2008; 50:9–16. [PubMed: 17876570]

24. Noebauer-Huhmann IM, Pinker K, Barth M, et al. Contrast-enhanced, high-resolution, susceptibility-weighted magnetic resonance imaging of the brain: dose-dependent optimization at 3 tesla and 1.5 tesla in healthy volunteers. Invest Radiol. 2006; 41:249–255. [PubMed: 16481907]

25. Schenck JF. The role of magnetic susceptibility in magnetic resonance imaging: MRI magnetic compatibility of the first and second kinds. Med Phys. 1996; 23:815–850. [PubMed: 8798169]

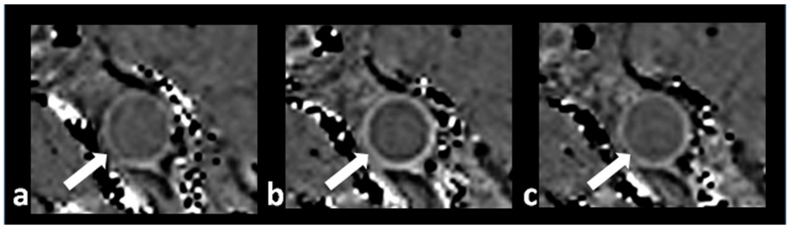

Figure 1.
Typical images from pre-contrast SWI (a), 1st contrast-enhanced SWI (b), and 2nd contrast-enhanced SWI (c). Images are shown at the same slice from one volunteer. Arrows indicate superficial femoral artery. Note the substantially improved vessel wall delineation in b.

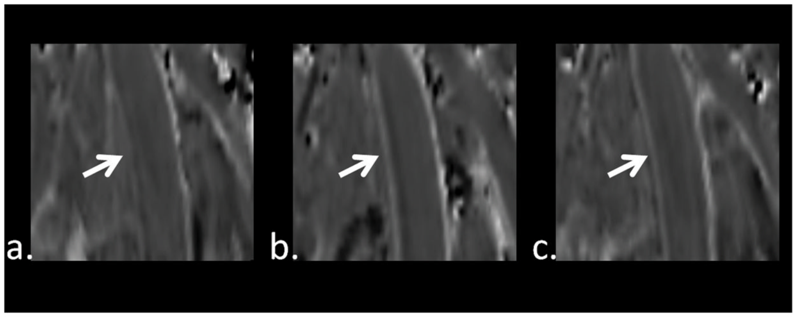

Figure 2.
MPR images from one volunteer from pre-contrast SWI (a), 1st contrast-enhanced SWI (b), and 2nd contrast-enhanced SWI (c). Arrows indicate superficial femoral artery. Note the substantially improved vessel wall delineation in b.

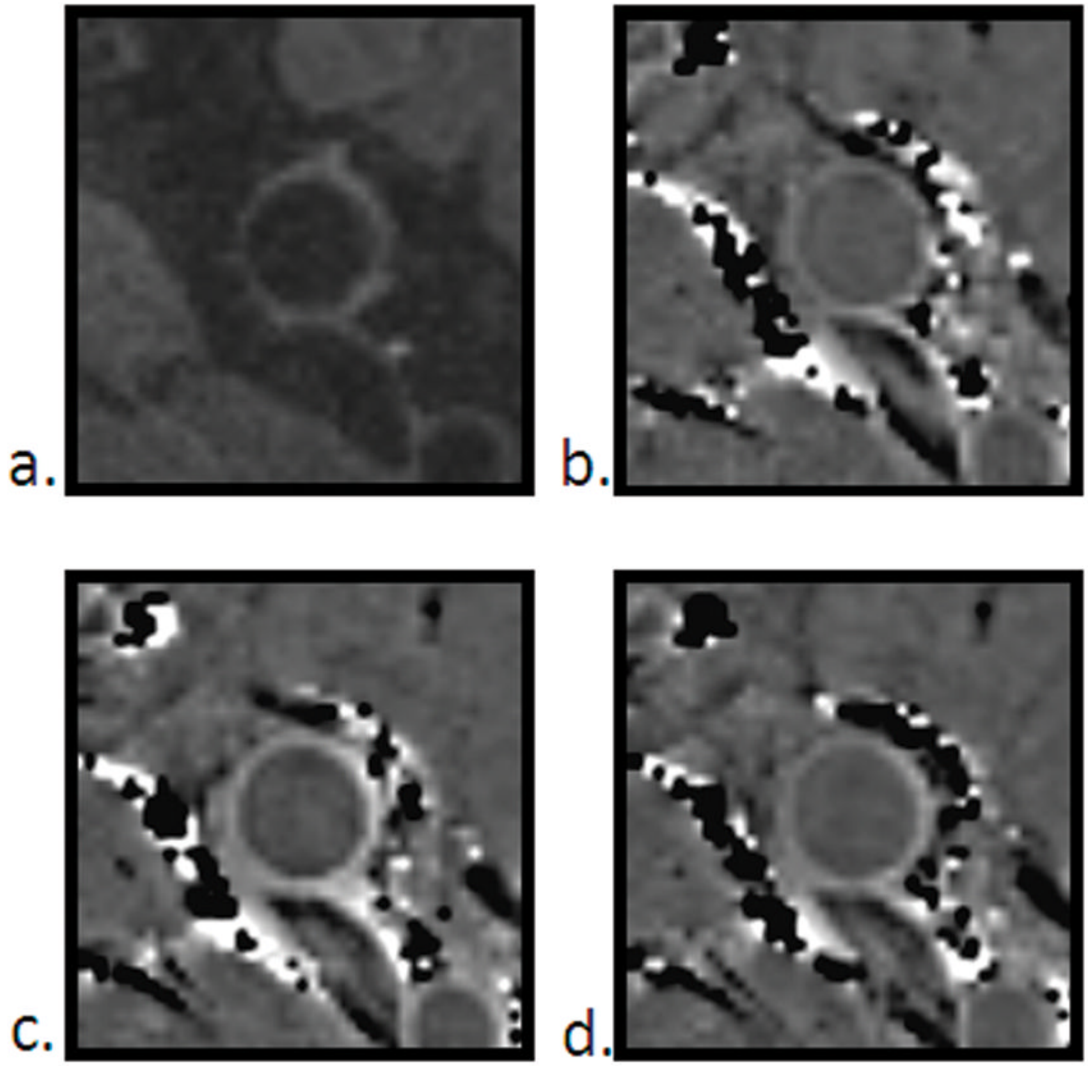

Figure 3.
Morphological comparison between TSE (a), pre-contrast SWI (b), 1st contrast-enhanced SWI (c) and 2nd contrast-enhanced SWI (d) images.

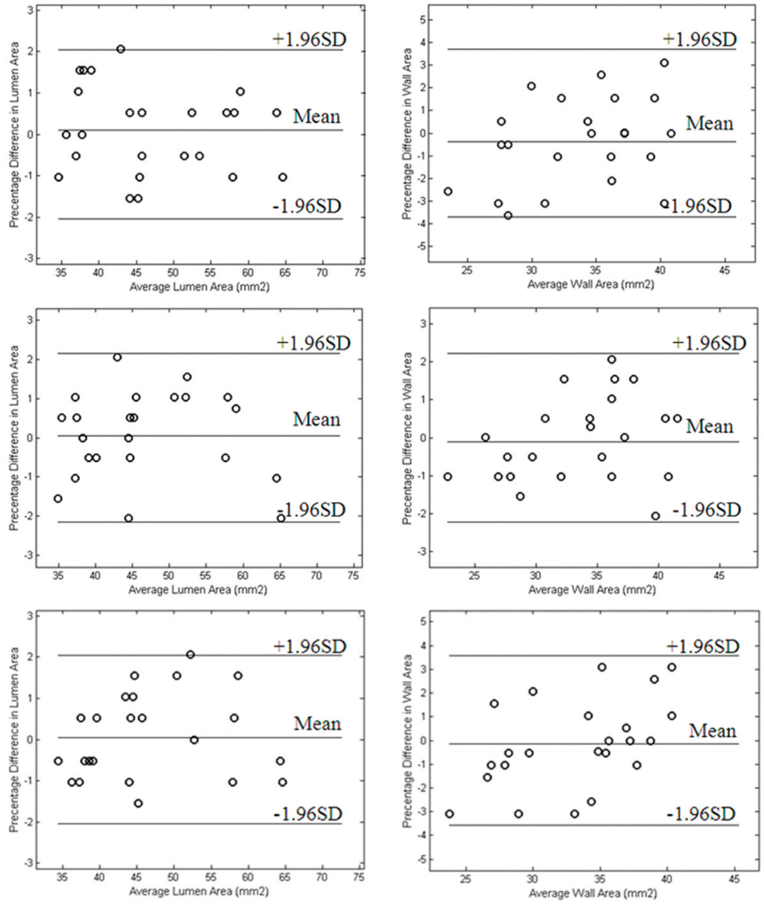

Figure 4.

Bland- Altman plots of area measurements of lumen (top left) and wall (top right) from TSE and pre-contrast SWI, lumen (middle left) and wall (middle right) from TSE and 1st contrast-enhanced SWI, and lumen (bottom left) and wall (bottom right) from TSE and 2nd contrast-enhanced SWI.

Table 1

Quantitative analysis of SWI lumen-wall contrasts. (n=220)

	Pre-contrast	1st Contrast-enhanced	2nd Contrast-enhanced
Phase Difference ($\Delta\phi$)	25.7°±6.3°	39.7°±7.6° ($p<0.001$)	25.3°±4.4° ($p=0.281$)
Phase CNR (CNR_{phase})	18.9±6.2	35.1±8.3 ($p<0.001$)	24.0±6.3 ($p<0.001$)

Note: Data are presented as mean ± standard deviation.